Analysis and Design of a Tubular Linear Permanent Magnet Servo Motor

*Yuanjiang Liu, G. P. Widdowson & S.Y. Ho.
ASM Assembly Automation Ltd, Watson Center, Kwai Chung, Hong Kong
Tel: 852-26192451 Fax: 852-26192159 *Email: John.liu@asmpt.com

Keywords

Finite Element Method, Linear Permanent Magnet Motor

Abstract

The analysis and design of a tubular linear PM servomotor is performed with emphasis on the optimisation of the motor envelope dimensions. In addition, constraints such as minimization of the force ripple and temperature rise are analysed using both electromagnetic and thermal finite element analyses. Control performance of the servo motor is demonstrated.

1. Introduction

An air cored permanent magnet tubular linear motor (PMTLM) offers significant advantages over conventional actuation technologies, since it exhibits a zero net radial force, assuming perfect assembly, has low copper loss, a high force/moving mass ratio and high efficiency[1]. These benefits make it an excellent choice for highly dynamic, reciprocal motion applications. Since the application presented here is of very high precision, the power dissipation and hence temperature rise must be minimized for a given dynamic operation. Also inherent of the motor in the operation, is to perform delicate force control, with force values two orders of magnitude less than the peak driving force. Hence, the cogging force generated must effectively be zero, constraining the design to a slotless variety. The design optimization will be presented, with empasis given to the electromagnetic and thermal finite element analyses that were used extensively throughout[2],[3].

2. PMTLM Structures

Fig. 1 shows a tubular slotless PM linear AC servomotor, where the windings are bonded to a yoke as a multi-pole stator and anisotropic NdFeB ring magnets are mounted on a mild-steel rod, which acts as a mover. Two different types of construction are illustrated. Firstly, type I is the conventional motor topology with surface mounted diametrically magnetized magnets, whilst type II is a Halbach magnetization structure, with an addational ring magnet added in the spacing of two magnets[4].

Where W_s ---- Coil axial thickness

W_m ---- Magnet axial length

W_p ---- Pole pitch

D_i ---- Magnet inner diameter

D_m ---- Magnet outer diameter

D_g , D_w ---- Coil inner/outer diameter

D_s ---- Stator sleeve outer diameter

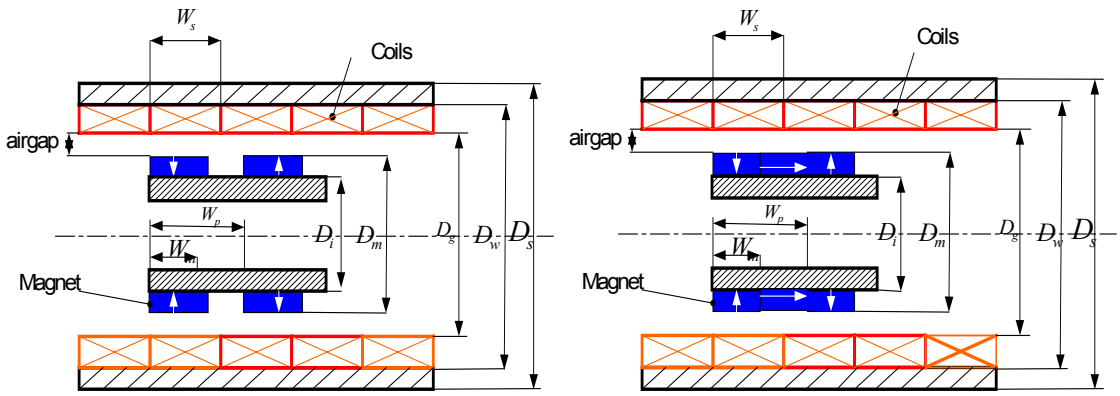

(a) Type I, Diametrically magnetized magnets (b) Type II, Halbach magnetized magnets

Figure 1 Simplified structure of a tubular slotless PM linear motor

3. Comparison between two types design

3.1 Analytical magnetic design.

The simulation of the force constant is essential in the design of a servo linear motor. To obtain rapid results that can be later verified by finite element analysis, a simple analytical technique was used to predict the airgap flux density[5] and force constant of the motor. They are expressed as

$$B(r) = \frac{1}{2r} \frac{B_r * (D_m - D_i)}{\ln(\frac{D_m}{D_i}) + \mu_r \ln(\frac{D_w}{D_m})}$$

$$\frac{Force}{current} = B(r)\Big|_{in\ winding\ area} * NL \qquad (1)$$

where NL is the total length of the conductor.

3.2 Analytical thermal design

So that the electromagnetic force from the motor could be predicted under the same temperature rise constraint, a simple analytical thermal model was used. In order to prevent demagnetization of the high energy NdFeB magnets, it was conservatively stated that the maximum temperature rise of the motor coil would be limited to $15^0 C$. In this system, since the motion is reciprocal, the maximum velocity is low and hence iron losses can be neglected. Therefore, the average temperature rise of the coil winding can be predicted from:

$$\Delta T = P_{cu}(i) * (\frac{1}{\alpha S_{cu}} + \frac{\delta_{ins}}{\lambda_{ins} S_{con}})$$

where $P_{cu}(i)$ is the total copper losses, α is the heat-transfer coefficient between the surface of motor and the surrounding air, S_{cu} is the area of close surface of motor, δ_{ins} is the total thickness of insulation layer and air layer, λ_{ins} is the equitant thermal conductivity of insulation layer and air layer, and S_{con} is the total contact area between the windings and the primary core.

Therefore, the rms current i could be predicted and substituted into (1) to predict the rms force capability of the motors.

3.3 Optimization

For the types of motor illustrated in Fig. 1, the pole width to pole pitch ratio plays an important role in determining the value of the force constant. Based on the same stator and winding construction, Fig. 2 shows the effect of varying this parameter. In the case of W_m / W_p=0.833 (W_m=10mm, W_p=12mm), the force constant can be increased 14% by employing a Halbach magnet. It will be increased 20% for the type II design with W_m / W_p=0.63 (W_m=8.53mm, W_p=13.4mm). It can be seen that the middle ring magnet with axial magnetisation strongly influences the force constant. Fig. 3 shows the force constant with respect to different radial heigths of middle ring magnet with the W_m=10mm, W_p=12mm.

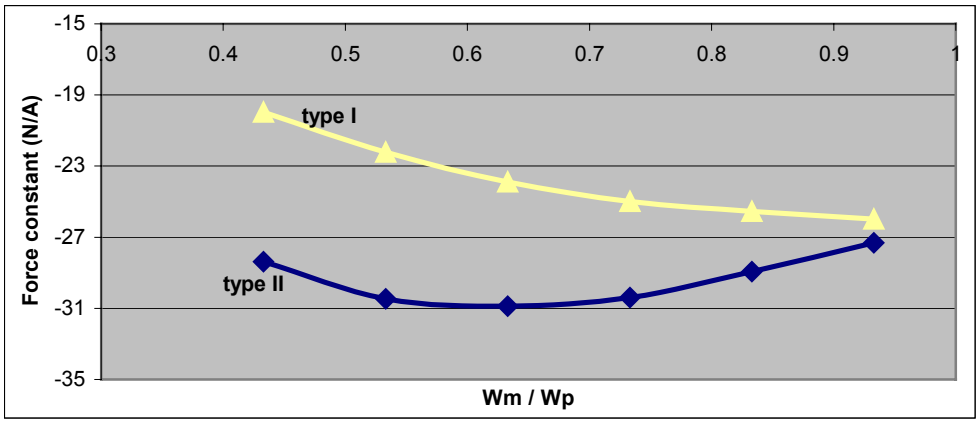

Figure 2 Variation of force constant with W_m / W_p

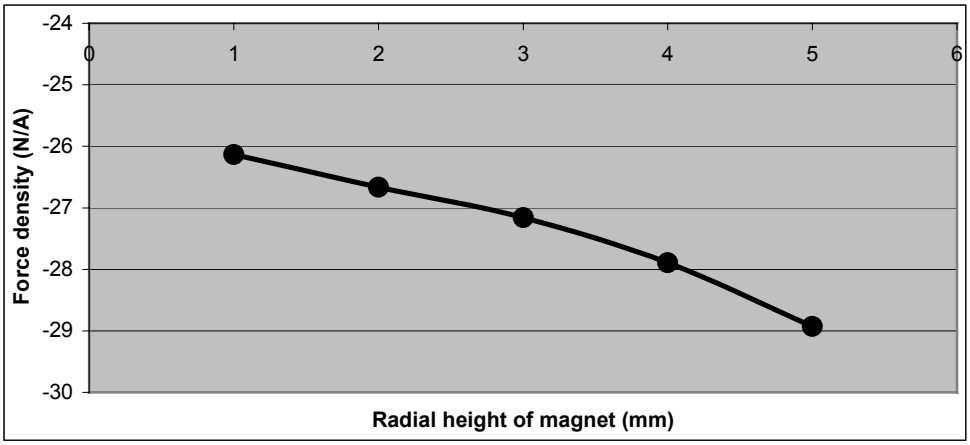

Figure 3 Force constant vs. radial height of magnet

3.4 Electromagnetic field finite element analysis

A 2D magnetostatic finite element package[2] was used to both determine the accuracy of the analytical solutions and to help in the optimization of the device. Fig. 4 shows the distribution of magnetic flux density and flux lines resulting from both the permanent magnets and the armature current, for both motor types with W_m=10mm and W_p=12mm. The flux density is below 1.8T in most of the magnetic circuit, except in the back-iron region A. In region A, the flux density is over 3T with Halbach magnets and the flux density is slightly below 3T without Halbach magnets. Such high magnetic fields can be tolerated when the velocity and hence electrical rotational velocity, is low.

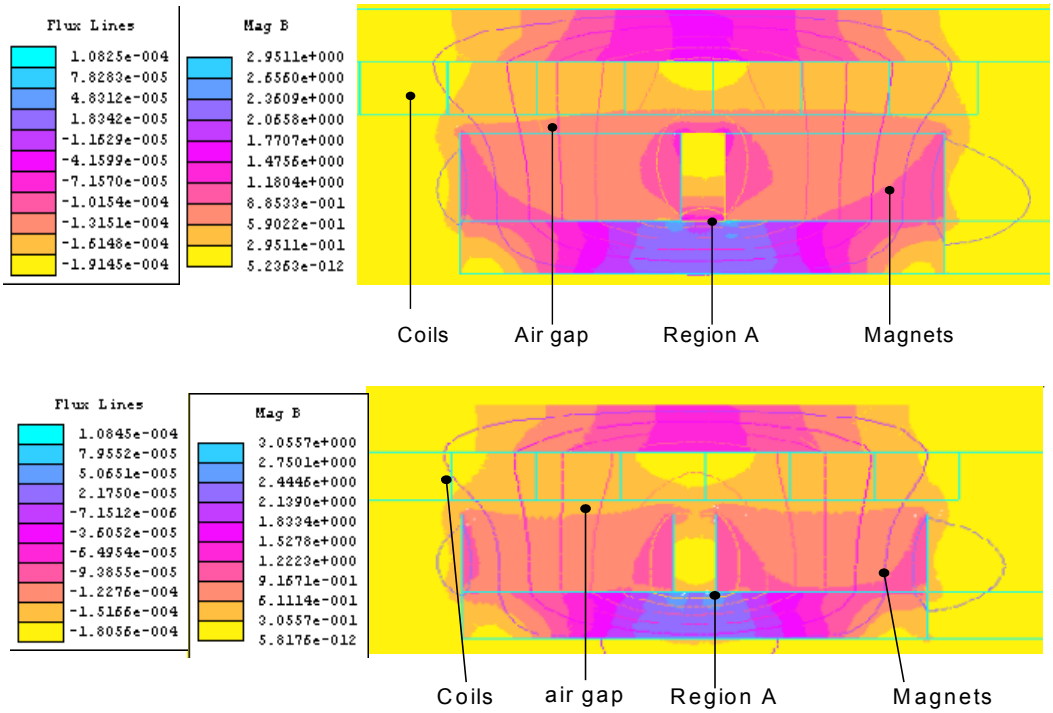

Figure 4 Flux lines distribution and flux density map (upper: type I, lower : type II)

Fig. 5 shows the radial flux density (Br) distribution in the center of the air gap over the mover. The magnetic field generaeted by the permanent magnet is the main component of air gap magnetic field. When only armature current is supplied, the flux density is almost zero.

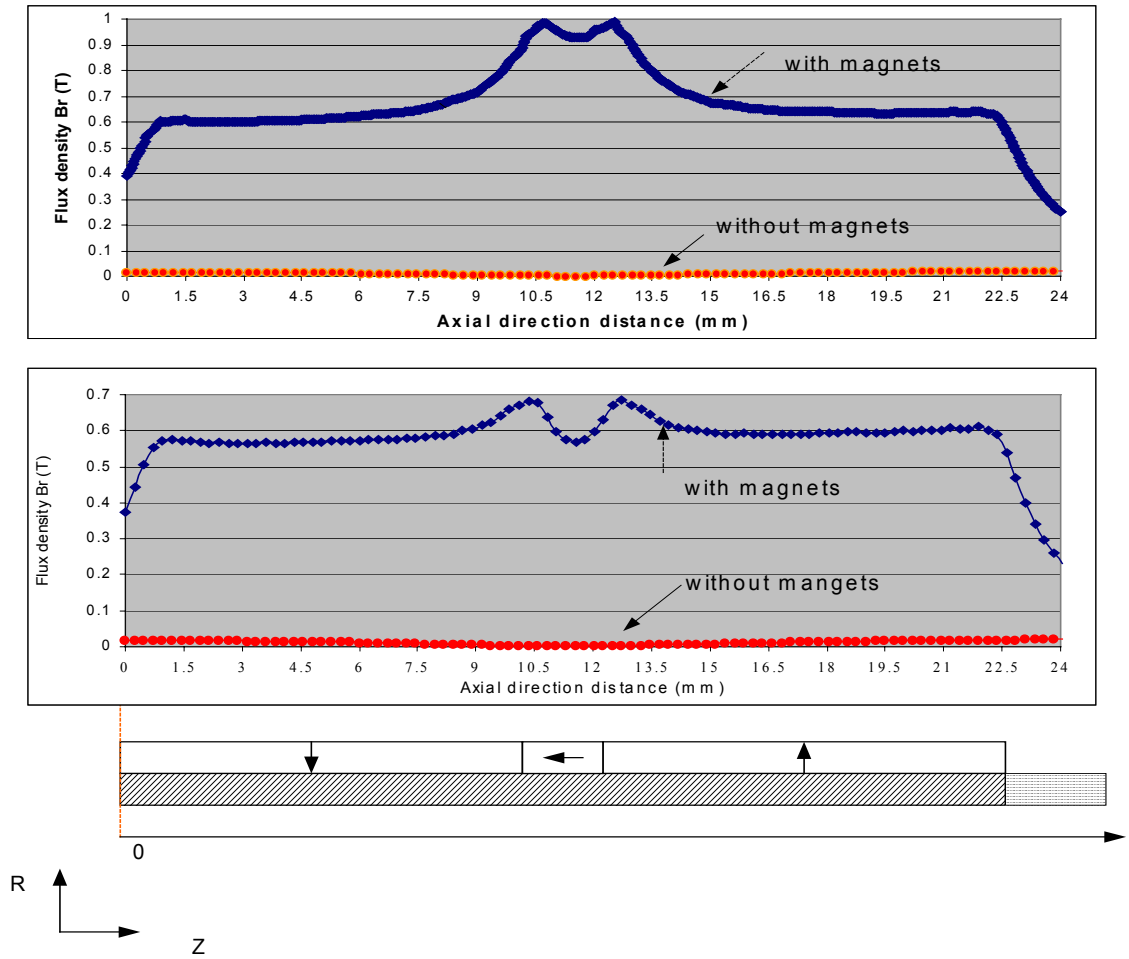

Figure 5 The radial flux density distribution(upper: type I, lower : type II)

3.5 Thermal finite element analysis

The linear motor system requires a low temperature rise of less than 15°C inside the core during operation. This is to prevent the demagnetization of the permanent magnet. The thermal analysis at steady-state was carried out to investigate the temperature profile within the whole motor system [3]. The following assumptions were introduced:

1) Contact between different parts are assumed to be perfect, without any contact resistance.
2) An air gap is modeled as a block of static air since the motor is studied at standstill operation.
3) Natural convection is assumed on the surfaces with a heat transfer coefficient =12 W/Km^2, ambient temperature=30 ^0C

Fig. 6 shows a thermal mapping of Type I motor under rated outputs. It is found that the maximum temperature rise is 15 ^0C at the mover of the motor. The temperature of the magnets is less 50 ^0C, avoiding demagnetization.

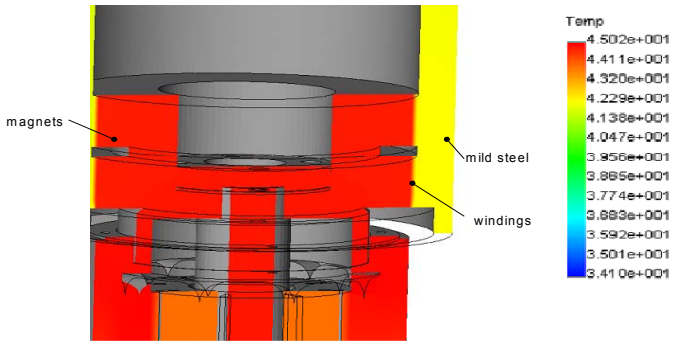

Figure 6 Distribution of the temperature at rated power dissipation

4. Experimental results

Although the Halbach arrangement clearly showed electromagnetic benefits over the conventional design, there were great difficulties in obtaining a stable assembly. Hence, so far, only experimental results from the type I motor will be presented here. Fig(7) shows a photograph of the assembled system.

The force constant was measured by applying a constant current through two phases of the motor. The results in Fig (8) show the average of the three readings(AB, AC and BC) and compare them with the theoretical prediction. It can be seen that although there is an offset, due to friction, the measurement corresponds closely with the prediction(3% error).

Fig(9) shows the temperature rise measurement of the motor when rms current is applied to the coils. The measurement was taken using thermocouples embedded into the motor and additionally placed on its surface. It can be seen that the temperature rise of $15\,^{0}C$ is close to the theoretical evaluation.

To ensure that the system is properly set up, prior to dynamic motion control tuning, the measurement of the current loop bandwidth and amplifier matching were undertaken. Fig(10) shows the current response from the system. The figure shows the output of the current with 10% peak input command. The -3dB current loop bandwidth, at approximately 3kHz, is sufficient for the application.

Fig(11) illustrates the position error of the motor, as measured from the linear encoder(command position – encoder position), for the most dynamic motion profile in this application. It shows that the maximum dynamic error is 5 μm and that the error quickly falls within a +/- 1 μm band.

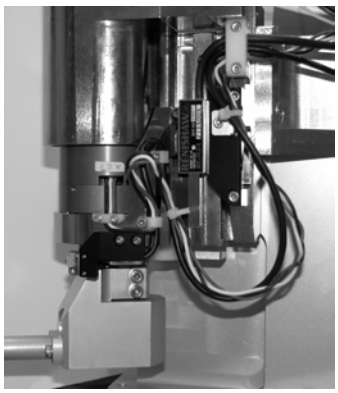

Figure 7 Photograph of assembled system

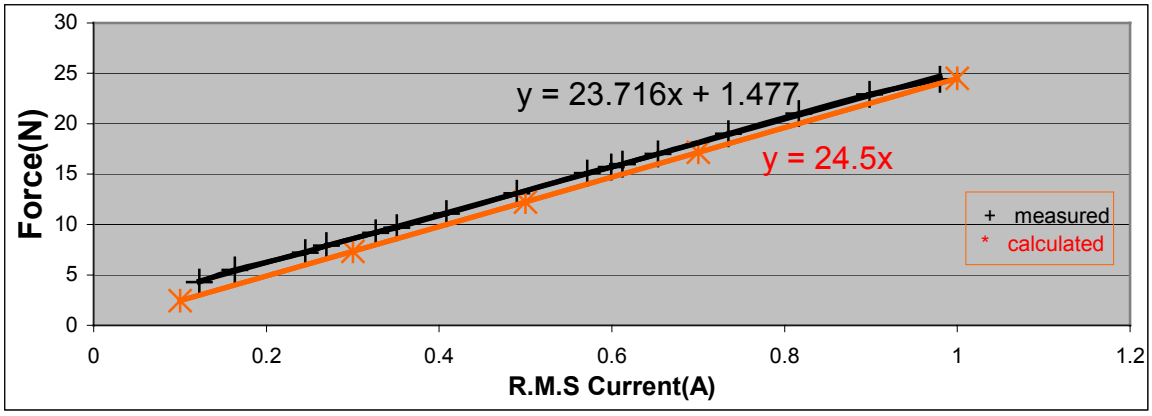

Figure 8 The force constant

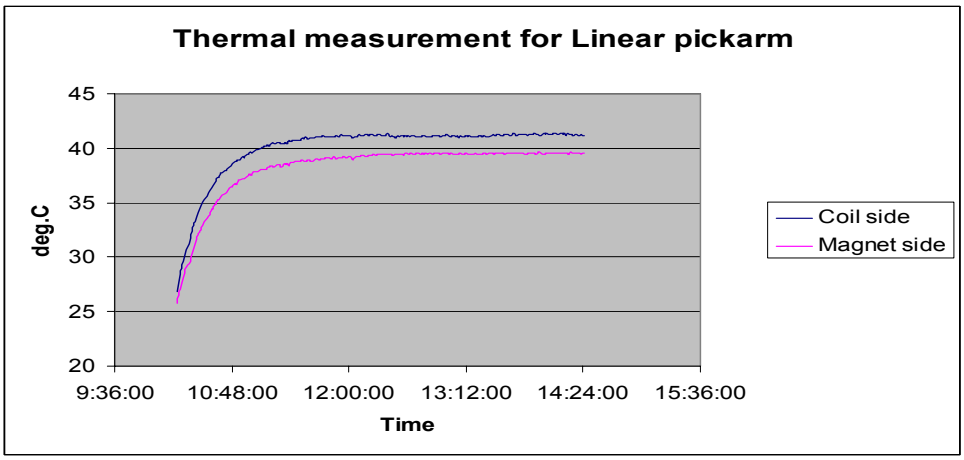

Figure 9 The temperature rise measurement

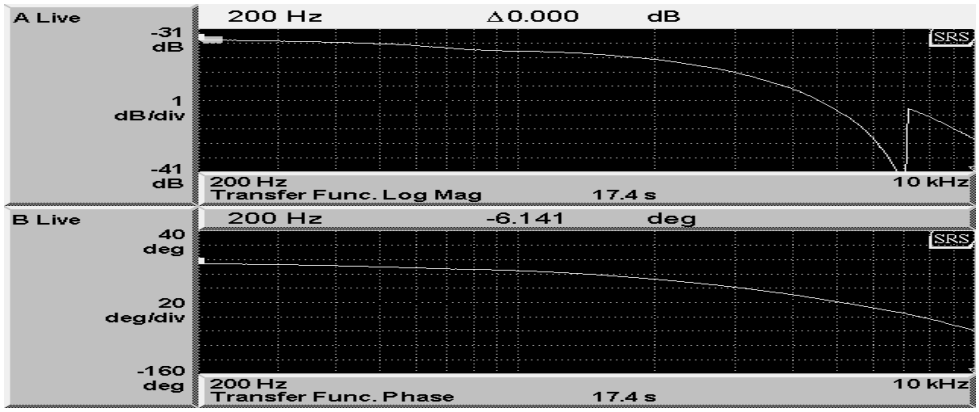

Figure 10 Current loop response of the motor

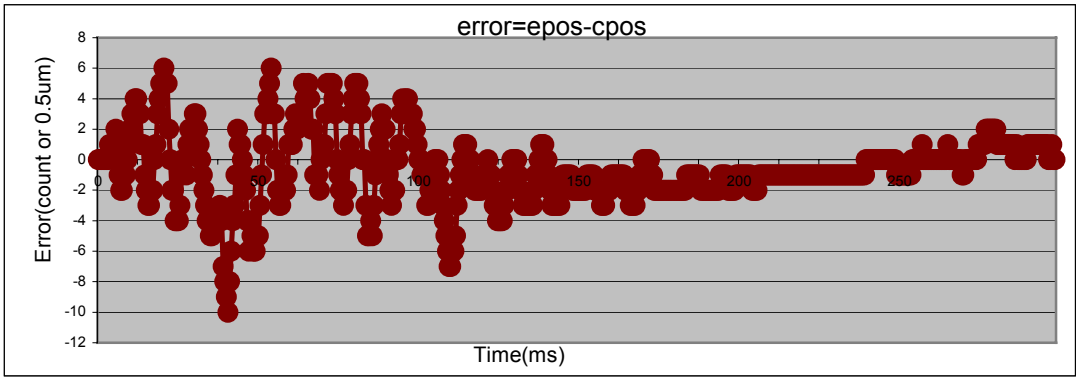

Figure 11 Dynamic and static position errors of the rotary system

5. Conclusions

A novel type of a slotless linear tubular permanet magnet motor has been proposed. Two alternative magnet topologies have been described in theory, although the Halbach structure could not, as yet, be realiseed in practice due to assembly difficulties. The motos were designed and optimised using a combination of analytical and finite element magneto-thermal techniques. The optimum design was manufactured and shown to agree closely with theoretical predictions and to exhibit exacting motion control performance. Future work will look into the design for manufacturing and optimisation of the Halbach magnet arrangement.

REFERENCES

[1] N Bianchi, etc, *Design Considerations for a Tubular Linear PM Motor for Servo Drives*. EPE Journal, 11(3), 2001,pp41-47.
[2] Ansoft Corporation, *Maxwell 2D field simulation*.
[3] Structural Research & Analysis Corporation, *COSMOS Design Star 4.0*.
[4] Z.Q.Zhu and D.Howe, *Halbach permanent magnet machines and applications: a review*. IEE Proc. Electr. PA, Vol.148, No.4, July 2001.
[5] K.Atalah, Z.Q.Zhu, J.K Mitchell, and D.Howe, *Curvature effects in radial-field permanent magnet machines*. Electric Machines and Power System, Vol.22, No.4, 1994, pp.511-520.